Discover Environment

RESEARCH Open Access

Modified ceramic filters as a local solution for Hg (II) and As (V) removal from polluted surface drinking waters

L. D. Senanu[1,2*], D. van Halem[1], G. Kranjac-Berisavljevic[2], S. J. Cobbina[2], B. E. Akorley[3] and S. G. J. Heijman[1]

*Correspondence:
lydiase2081@uds.edu.gh

[1] Delft University of Technology, P. O. Box 5048, 2600 GA Delft, the Netherlands
[2] Nyankpala Campus, University for Development Studies, P. O. Box TL 1882, Tamale, Ghana
[3] C.K. Tedam University of Technology and Applied Sciences, Navrongo, Ghana

Abstract

Unregulated mining activities can pollute surface drinking water sources with toxic metals such as arsenic and mercury, creating serious environmental and public health concerns in resource-limited communities. In this study, locally fabricated ceramic water filters prepared from clay and different biosorbents were evaluated for the removal of As(V) and Hg(II) from contaminated water. Three ceramic formulations were produced using rice husks, sheanut shells, and groundnut shells as pore-forming and functional biosorbent additives. Batch adsorption and full-pot filtration experiments were conducted to determine removal efficiency, the effects of initial concentration, contact time, and adsorbent dosage, as well as the practical filtration performance of the developed filters. Structural characterization using X-ray diffraction (XRD) and Fourier transform infrared spectroscopy (FTIR) showed that the sheanut-shell-based material (CMS) possessed a higher amorphous fraction and smaller crystallite domains, features that are favorable for adsorption. Among the tested materials, CMS exhibited the best performance, achieving a maximum Hg(II) removal efficiency of 80.7% at an initial concentration of 0.5 mg/L under the tested conditions. Kinetic data were better described by the pseudo-first-order model ($R^2 \geq 0.99$), while equilibrium data were best fitted by the Freundlich isotherm model ($R^2 \geq 0.99$), indicating adsorption on heterogeneous surfaces. Under filtration conditions, mercury removal was consistently higher than arsenic removal, with CMS showing the best overall performance. These findings demonstrate that biosorbent-modified ceramic water filters, particularly those incorporating sheanut shells, offer a promising low-cost and locally deployable option for the treatment of mining-impacted water.

Keywords: Ceramic water filter, Arsenic, Mercury, Drinking water, Illegal mining

1 Introduction

The contamination of surface and groundwater by toxic heavy metals such as arsenic (As) and mercury (Hg) is a significant global environmental and public health challenge. Arsenic contamination is widespread and has been reported in several countries, posing severe health risks due to its high carcinogenic potential [1,35,36]. The World Health

Organization (WHO) has classified arsenic as a Group I human carcinogen and set a stringent limit of 0.01 mg/L in drinking water to mitigate its toxic effects. Mercury pollution, primarily stemming from industrial and anthropogenic activities, exists in three forms: elemental mercury (Hg^0), monovalent mercury (Hg^+), and divalent mercury (Hg^{2+}), with Hg^{2+} being the most toxic [2,37]. Chronic exposure to mercury is linked to severe health conditions, including neurological damage, kidney failure, gastrointestinal distress, and cardiovascular diseases [2,38]. Alarmingly, unsafe drinking water contributes to substantial global mortality, with over 400,000 childhood deaths annually attributed to waterborne contaminants [3,39,42]. The burden of this crisis disproportionately affects low- and middle-income countries, where access to clean water remains a persistent challenge [40,41]. In Ghana, heightened mining operations have damaged the environment, as mining activities undertaken by these small-scale mining and "galamsey" operators have resulted in the destruction of forest cover, agricultural lands and the pollution of water bodies[4–6]. According to [7] tests done on some rivers in the South-Western basin of Ghana revealed the following levels of heavy metals: Hg (10–7160 µg/L); Pb (10–1580 µg/L); Cd (3–12,413 µg/L); As (10–9900 µg/L) in the water column. Arsenic is a metalloid found everywhere from the soil, natural water bodies and rocks [8]. Human activities coupled with natural phenomenon causes arsenic to be mobilized in the environment [8]. Since they are found in rocks, blasting during mining operations releases them into the environment. The presence of arsenic in natural and ground water is a global phenomenon, which has been reported in several countries [9–11]. Sources of arsenic pollution stem from both natural (biological activity, geochemical reactions, weathering processes and volcanic emissions) and human activities (mining, metal and ammunition industries, cement and glassware production) [12,13]. Arsenic can be found in various forms depending on environmental conditions present especially pH [13]. Under aerobic conditions, arsenic is present as arsenate (As (V)) whiles in anaerobic conditions, arsenite (As (III)) is present [10,13–15]. Monomethyl arsenate and dimethyl arsenate are the organic species of arsenic [13]. The most toxic form of arsenic is arsenite and it has more mobility than arsenate [13] and very difficult to remove from water [16]. Under pH values 6–9, arsenic is highly mobilized under both reducing and oxidizing conditions [17]. Mercury is a heavy metal, which occurs naturally in the environment [16]. The forms of mercury found in the environment; Hg (0), Hg (I) and Hg (II) and the most toxic form is Hg (II) [2]. Environmental factors will affect the type of mercury species that will be available in natural waters at a time [16]. The mercury species that may be found in natural waters are elementary mercury (Hg (0)), mercuric mercury (Hg (II)) and methylated mercury (MeHg, DMHg) [2]. Due to mercury's high vapor pressure, gaseous elementary mercury is the main form of mercury in the atmosphere. The presence of mercury in aquatic systems is usually by runoffs from watershed and deposits from the atmosphere [16]. Sources of mercury are both natural and anthropogenic and the natural sources include volcanic emissions, geothermal activity and evaporation of mercury from the soil [2,16]. Anthropogenic sources include mining (gold mining), coal fired combustions, chemical industries and waste incinerators [2,16]. The re-emission of mercury is another source of mercury pollution in the environment. This source of pollution initially starts as a natural phenomenon, which deposits mercury in water or soil but become agitated again through human or forces of nature.

Conventional water treatment technologies, including ion exchange, chemical precipitation, electrochemical treatment, and reverse osmosis, are effective but often hindered by high operational costs, infrastructure demands, and complex maintenance requirements [18,19,49]. These limitations render them impractical for resource-constrained settings, necessitating the exploration of cost-effective, efficient, and locally available alternatives. Adsorption-based treatment has emerged as a promising approach due to its affordability, simplicity, and efficiency in removing a broad spectrum of contaminants [19,20,48,50].

Ceramic water filter (CWF) is a water treatment product that combines clay and burnable materials to provide a filtering system to remove pathogen and solids from polluted water [21,44,45]. The use of locally sourced materials in its production makes it a potential method that can support in achieving SDG 6.1 in the shortest possible time. The CWF is designed into various forms like the candle filter and the porous pot filter [22,23]. The burnable material is usually agricultural waste like rice husks and sawdust which burn out during the firing period to create pores, which reject the passage of solids and pathogens [23]. Some factories provide a bactericide coating to give it extra protection in removing pathogens [22]. This treatment method has gained high interest globally among researchers, in its potential to remove more than just pathogens and solids [43,44].Ceramic water filters are mainly known for treating pathogen-infected water sources for drinking water purposes [45]. Their ability to remove other pollutants apart from microbes has not been extensively explored. An experiment conducted with clay membranes made with sawdust and clay soil, was reported to have removal efficiency of 99–100% for Pb^{2+}, 100% for Cd^{2+} and 97–100% for Cu^{2+}[24]. During the experiments, the author noted that at pH 7 and 9, removal was very high indicating the reactions were favorable in alkaline conditions. In Colombia, [25]conducted the removal of arsenic, lead and mercury with ceramic pot filter made with clay and sawdust. In addition to the clay filter pot, [25]added a separate adsorption column comprising of zeolite and activated carbon. Results showed that, with the addition of the zeolite-activated carbon column, removal efficiencies for mercury moved from 91.5% to 92.5%, 92.1% to 98.1% for lead. However, arsenic removal showed quite low results, i.e. 50.2% to 52.3% when the zeolite-activated column was added to the CWF. The possible explanation for this observation according to the author the significant arsenic removal is observed in mainly acidic conditions (pH 5–6), however, the experiments were carried under neutral conditions and that is why the low removal efficiency for arsenic was observed. The addition of inorganic additives like hydroxyapatite to ceramic water filters saw the increased removal of lead from aqueous solutions [26]. In contrast, ceramic water filter without additives observed very low removal efficiencies for lead. This is indicative of the fact that, for ceramic water filters cannot effectively remove chemical pollutants without some form of modification. Research by [46], indicated that the use of single and double ceramic designed filter, As(V) was removed up to 86%.Chitosan coated ceramic membranes were used to remove almost 100% mercury [47]. Cerium oxide coated CWF made from clay and rice husks was reported to have arsenic removal efficiency move from 61.93% to 84.58% as the amount of the cerium oxide coating increased from 0 to 1.0 g/L [27]. Factors influencing this observation include the pH and initial arsenic concentration. Inadequate surface-active sites for adsorption was responsible for decreased removal

as the initial arsenic concentration was increased [27]. In addition, for lower pH values, removal efficiency of arsenic was high with cerium oxide whiles higher pH values showed a decline in the removal of arsenic. At alkaline pH, both cerium oxide and arsenic are negatively charged therefore repulsing each other and preventing the removal of arsenic. It is important to note that more research is needed where chemical removal with CWFs made with different biosorbents other than sawdust, as well as the incorporation of other adsorbents to thoroughly understand the reaction mechanisms involved in the removal of chemical pollutants from aqueous solutions. In addition, experimentations with different biosorbents could provide information on the effects of biosorbents on the removal of chemical pollutants since different biosorbents have different functional groups, which could enhance pollutants removal.

The novelty of this study lies in the incorporation of locally available agricultural waste materials, specifically sheanut shells and groundnut shells, into ceramic water filters to enhance the simultaneous removal of both cationic Hg(II) and oxyanionic As(V). While ceramic pot filters are widely recognized for pathogen removal, their application for toxic metal removal remains underexplored, particularly using alternative biosorbents beyond conventional sawdust or rice husks. This approach therefore provides a low-cost, locally sourced, and potentially scalable water treatment option for mining-affected and resource-constrained communities.

By evaluating the adsorptive performance, physicochemical interactions, and practical feasibility of modified ceramic filters, this research contributes to the development of a locally sourced and easily deployable water treatment technology. The study not only addresses the fundamental limitations of conventional methods but also aligns with global efforts to achieve Sustainable Development Goal 6 (SDG 6): Clean Water and Sanitation for All.

2 Materials and methods

2.1 Material synthesis

2.1.1 Chemical and reagents

All chemicals used in the study were of analytical grade and were used without further purification. Deionized water with resistivity of 18 MΩ cm, obtained from a Milli-Q water purification system, was used for the preparation of all standard solutions. Stock standard solution of arsenic (As(V)) and mercury (Hg(II)) (1000 mg/L) were used to prepare working solutions of desired concentrations by serial dilution. Synthetic Hg(II) and As(V) solutions were prepared to simulate contaminated surface waters commonly encountered in mining-affected regions. A 10 mM sodium bicarbonate ($NaHCO_3$) buffer and 5 mM sodium chloride (NaCl) were prepared to maintain the ionic strength and pH of the experimental solutions. The addition of sodium chloride (5 mM) was to maintain ionic strength during the experiments; at this relatively low concentration, chloride complexation of Hg(II) may occur to a limited extent but is not expected to dominate the overall adsorption behavior. In this experiment, we modified the existing ceramic water filter (CWF) by adding sheanut shells, and groundnut. Details are presented below in Table 1.

Table 1 Various designs of ceramic material designs used in the study

Type of MCWF materials	Biosorbent (kg)	Terracotta clay (kg)	Kaolin clay (kg)	Dry mass before firing (kg)	Dry mass after firing (kg)
CMR	Rice husks (4)	4	9.5	9.20	7.31
CMS	Sheanut shells (4)	4	9.5	9.12	6.98
CMG	Groundnut shells (4)	4	9.5	9.25	7.27

2.1.2 Manufacturing of ceramic pot filters

The ceramic pot filters were locally fabricated by mixing the different raw materials with adequate water, as presented in Table 1, and subsequently firing the formed materials in a kiln at 850 °C. For the batch adsorption experiments, the ceramic materials were designated as follows:

a. CMR–Ceramic water filter material with rice husks
b. CMS–Ceramic water filter material with sheanut shells
c. CMG–Ceramic water filter material with groundnut shells

The mass variation of the ceramic water filter materials before and after firing is presented in Table 1. The dry mass decreased for all formulations after firing at 850 °C, reflecting the combustion of organic matter and loss of moisture. The CMS (sheanut-shell) material recorded the highest mass loss of 2.14 kg (23.46%), followed by CMG (groundnut-shell) with 1.98 kg (21.41%), while CMR (rice-husk) exhibited the lowest mass loss of 1.89 kg (20.54%).

The relatively higher weight reduction in the sheanut-shell material suggests a greater proportion of volatile components, which likely generated a more porous structure upon firing. In contrast, the rice-husk material retained more mass, possibly due to its higher silica content, resulting in a denser and mechanically stronger matrix. The groundnut-shell material displayed intermediate characteristics, indicating a balanced combination of porosity and structural integrity. These differences in mass loss are indicative of the varying organic and ash contents of the biosorbents, which directly influence the porosity, strength, and filtration performance of the resulting ceramic water filters.

2.2 Experimental design

2.2.1 Adsorption capacity

To determine the effect of initial adsorbate concentration, As(V) and Hg(II) solutions with varying concentrations (0.25 mg/L, 0.5 mg/L, 2.0 mg/L, 5.0 mg/L, and 10 mg/L) were prepared. Each solution contained 10 mM $NaHCO_3$ buffer and 5 mM NaCl. For this experiment, 0.1 g of crushed ceramic pot materials (CMR, CMS, and CMG) were used as adsorbents. To investigate the effect of adsorbent weight, varying masses (0.02 g, 0.04 g, 0.06 g, 0.08 g, and 0.1 g) of CMR, CMS, and CMG were added to 0.5 mg/L As(V) and Hg(II) solutions, also containing 10 mM $NaHCO_3$ buffer and 5 mM NaCl. For the effect of contact time, 0.1 g of each adsorbent (CMR, CMS, and

CMG) was added to 0.5 mg/L As(V) and Hg(II) solutions. The contact times investigated were 1 h, 4 h, 8 h, 12 h, and 24 h. To evaluate the full pot experiment, As(V) and Hg(II) solutions with concentrations of 0.5 mg/L and 5 mg/L were prepared with 10 mM $NaHCO_3$ buffer and 5 mM NaCl. These solutions were filtered through ceramic water filters (CWFR, CWFS, and CWFG) at contact times of 0 h, 1 h, 4 h, 8 h, 12 h, and 24 h. All filtrates were analyzed using Hydride Vapor Generation Atomic Absorption Spectroscopy (HVG-AAS).

2.3 Data analysis

The adsorption performance of the ceramic materials was evaluated using removal efficiency, adsorption capacity, kinetic models, and adsorption isotherm models.

The removal efficiency of Hg(II) and As(V) was calculated using Eq. (1):

$$\mathrm{Re}moval(\%) = \frac{C_0 - C_e}{C_0} \times 100 \tag{1}$$

The equilibrium adsorption capacity was calculated using Eq. (2):

$$q_e = \frac{(C_0 - C_e)V}{m} \tag{2}$$

where C_0 and C_e are the initial and equilibrium concentrations of the adsorbate, respectively (mg L^{-1}); V is the volume of the solution (L); and m is the mass of adsorbent used (g).

The pseudo-first-order and pseudo-second-order kinetic models were used to describe the adsorption kinetics. Their linearized forms are given in Eqns. (3) and (4), respectively:

2.3.1 Pseudo-first-order

$$\ln(q_e - q_t) = \ln q_e - k_1 t \tag{3}$$

2.3.2 Pseudo-second-order

$$\frac{t}{q_t} = \frac{1}{k_2 q_e^2} + \frac{t}{q_e} \tag{4}$$

where q_t is the adsorption capacity at time t(mg g^{-1}), q_e is the adsorption capacity at equilibrium (mg g^{-1}), k_1 is the pseudo-first-order rate constant (min^{-1}), and k_2 is the pseudo-second-order rate constant (g mg^{-1} min^{-1}).

To describe equilibrium adsorption behavior, the Langmuir, Freundlich, and Temkin isotherm models were applied.

2.3.3 Langmuir isotherm

$$q_e = \frac{q_{\max} K_L C_e}{1 + K_L C_e} \tag{5}$$

where $q_{\max}$ is the maximum adsorption capacity (mg g^{-1}) and K_L is the Langmuir constant (L mg^{-1}).

2.3.4 Freundlich isotherm

$$q_e = K_F C_e^{1/n} \tag{6}$$

where K_F is the Freundlich adsorption constant and $1/n$ is the heterogeneity factor.

2.3.5 Temkin isotherm

$$q_e = \frac{RT}{b_T} \ln (A_T C_e) \tag{7}$$

where R is the universal gas constant (8.314 J mol^{-1} K^{-1}), T is the absolute temperature (K), b_T is the Temkin constant related to the heat of adsorption, and A_T is the Temkin equilibrium binding constant. In addition to the coefficient of determination (R^2), the sum of squared errors (SSE) was used to further assess the goodness-of-fit of the kinetic and isotherm models.

3 Result and discussion

3.1 Characteristics of the filter material

The XRD patterns of CMS, CMG and CMR are presented in Fig. 1a. All samples exhibit distinct differences in their diffraction profiles, reflecting variations in phase composition, crystallite size and degree of structural order. The sample labeled CMR displays sharp and intense peaks, particularly near $2\Theta \approx 28°$, indicating a high degree of crystallinity. In contrast, CMG exhibits moderately intense and less sharp peaks, signifying a semi-crystalline structure. CMS, however, reveals broad and weak diffraction peaks, characteristic of a predominantly amorphous material with poor long-range order.

These variations in peak sharpness and intensity suggest differences in crystallite sizes, which can be qualitatively interpreted using the Scherrer equation. The narrow peaks observed in CMR suggest the presence of relatively large crystallites, whereas the broader peaks in CMS indicate smaller crystallite domains or amorphous regions. CMG exhibits intermediate characteristics. The smaller crystallites in CMS are typically associated with higher surface areas, which are beneficial for surface-based applications such as adsorption.

In terms of percentage crystallinity, the samples follow the trend: CMR > CMG > CMS. The crystalline fraction was estimated qualitatively based on the ratio of the area under crystalline peaks to the total area (crystalline + amorphous). CMR exhibits a crystallinity greater than 70%, CMG falls within 40–60%, and CMS is below 30%. These findings suggest that CMS is structurally less ordered, with a significant amorphous phase that is generally rich in defect sites and reactive functional groups (e.g., surface hydroxyls).

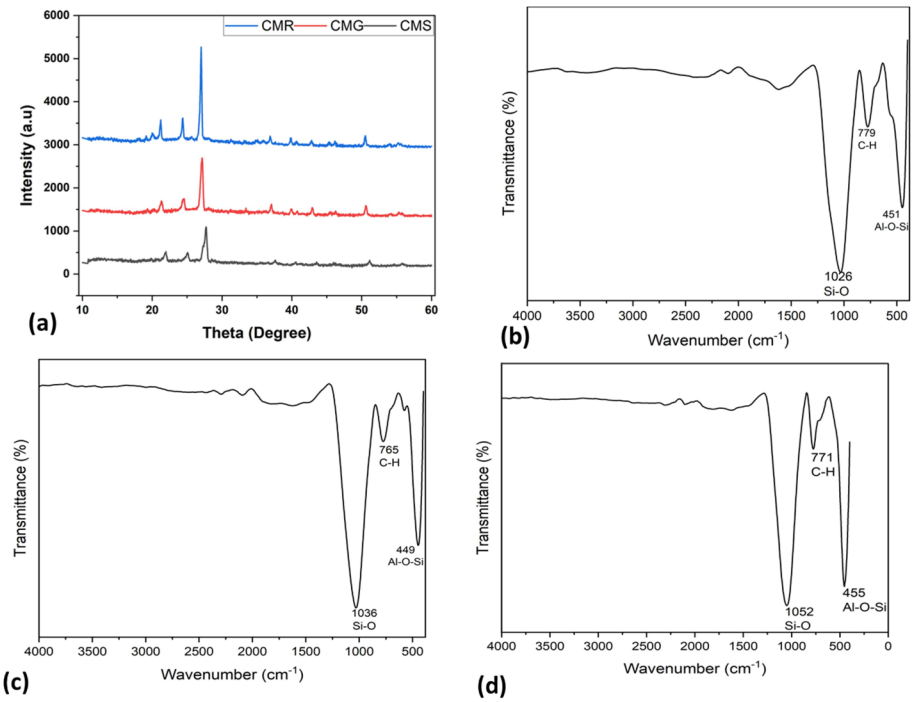

Fig. 1 **a** XRD patterns for CMR, CMG and CMS, **b** The Fourier Transform Infrared Spectroscopy of CMR, **c** The Fourier Transform Infrared Spectroscopy of CMS and **d** Fig. 2c. The Fourier Transform Infrared Spectroscopy of CMG

Such features are particularly favorable for adsorptive interactions with toxic heavy metals. The structural characteristics of the materials strongly influence their adsorption potential for arsenic (As) and mercury (Hg). CMS, with its high amorphous content and small crystallite size, is expected to exhibit superior adsorption performance. The abundant structural defects, increased surface area, and possible presence of uncoordinated oxygen species enhance its capacity to bind As and Hg ions through mechanisms such as surface complexation, ion exchange, and electrostatic interactions. CMG, with moderate crystallinity, offers a balanced structure that may support reasonable adsorption performance, though lower than CMS. In contrast, the highly crystalline CMR, while structurally stable, possesses fewer reactive surface sites, thereby limiting its inherent adsorption capacity for these contaminants unless modified. Conclusively, CMS demonstrates the most favorable structural attributes for efficient adsorption of arsenic and mercury, making it a promising candidate for water treatment applications targeting these priority pollutants.

The FTIR spectroscopy was used to examine the molecular structure and surface functional groups of the ceramic adsorbents. The spectra of CMR, CMS, and CMG are presented in Fig. 1b–d. In all samples, the strong absorption bands observed in the range of 1026–1052 cm^{-1} are attributed to Si–O stretching vibrations, confirming the silicate framework of the clay-based ceramic matrix. Bands observed in the region of 449–455 cm^{-1} are assigned to Al–O–Si bending vibrations, indicating the presence of aluminosilicate structures. The bands in the 765–779 cm^{-1} region may be associated with lattice vibrations of silicate phases and related structural modes within the ceramic

framework. In all, the FTIR spectra confirm that the fabricated materials are dominated by silicate and aluminosilicate bonding environments, which are important for surface interaction with metal contaminants.

3.2 Comparative behavior of the adsorption potentials of CMR, CMS and CMG

3.2.1 Effect of initial time

The effect of contact time on the adsorption of Hg(II) and As(V) by CMR, CMS, and CMG is presented in Fig. 2a and b. All three adsorbents exhibited a rapid increase in removal efficiency during the initial stage of adsorption, indicating the availability of abundant active sites and favorable initial adsorbate–adsorbent interactions. As contact time increased, the rate of adsorption gradually slowed and approached equilibrium, suggesting progressive occupation of the available surface sites.

For As(V), the three adsorbents showed gradual improvement in removal with increasing time, after which the adsorption tended toward a plateau as equilibrium was approached. CMS showed the highest final removal efficiency, slightly exceeding those of CMR and CMG. For Hg(II), all adsorbents exhibited substantially higher removal efficiencies than for As(V), with near-equilibrium values attained after prolonged contact time. Among the materials, CMS showed the best Hg(II) removal performance, reaching 80.7%, while CMR and CMG achieved 78.4% and 76.6%, respectively. The superior performance of CMS suggests that its higher amorphous content and more reactive surface sites favored heavy metal uptake.

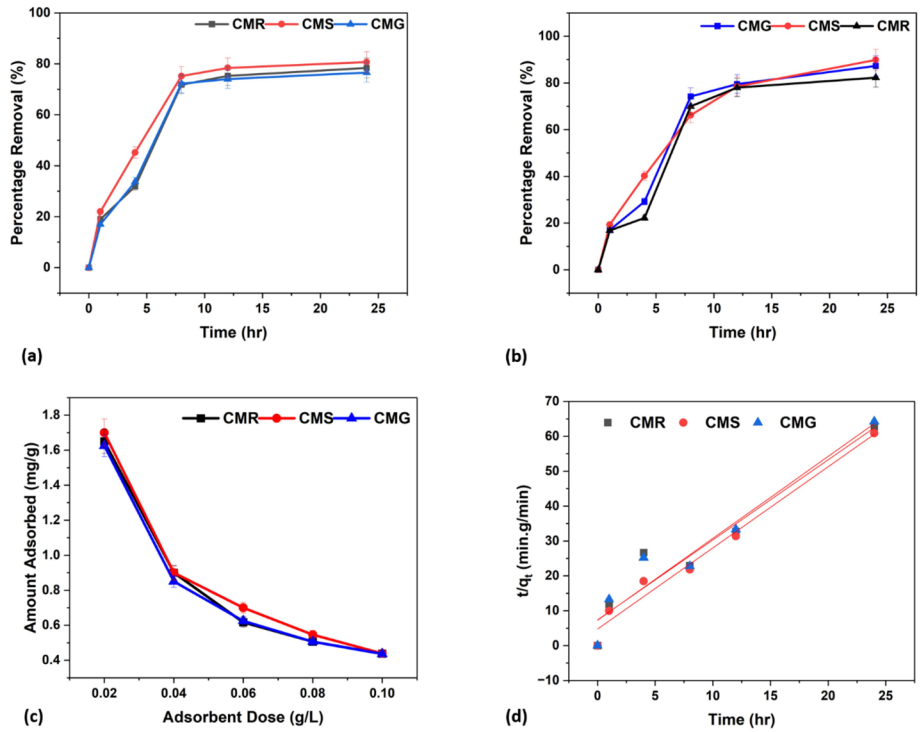

Fig. 2 **a** Removal efficiency of CMR, CMS and CMG with Hg (II), **b** Removal efficiency of CMR, CMS and CMG with As (V), **c** Adsorption capacity of CMR, CMS and CMG with Hg (II) and **d** Kinetic plot of CMR, CMS and CMG with As (V)

3.2.2 Effect of the adsorbent dosage

The effect of adsorbent dosage on Hg(II) and As(V) removal was evaluated by adding 0.02, 0.04, 0.06, 0.08, and 0.10 g of CMR, CMS, and CMG to 100 mL (0.1 L) of 0.5 mg L^{-1} metal ion solution. The results are presented in Fig. 2c, where the x-axis represents the adsorbent dose (g) and the y-axis represents the removal efficiency (%).

As the adsorbent dosage increased, the removal efficiency of Hg(II) and As(V) generally increased for all adsorbents. For Hg(II), removal efficiency increased from approximately 65–68% at 0.02 g to 87–88% at 0.10 g, depending on the adsorbent type. The improvement in removal efficiency with increasing dosage is attributed to the greater availability of adsorption sites and larger surface area, which enhance the probability of interaction between metal ions and the adsorbent surface. Similar trends have been widely reported for adsorption systems involving heavy metals and metalloids [28,29].

In contrast, the adsorption capacity expressed as mg g^{-1} decreased with increasing adsorbent dosage. This phenomenon is commonly attributed to the partial underutilization of adsorption sites at higher adsorbent masses, where the available adsorption surface exceeds the amount of contaminant present in solution. Consequently, although the total amount of contaminant removed from solution increases, the uptake per unit mass of adsorbent decreases due to unsaturated adsorption sites and reduced adsorbent utilization efficiency [28].

Considering the higher removal efficiencies achieved at larger adsorbent dosages, 0.10 g was selected as the optimum adsorbent mass for subsequent experiments. At this dosage, the highest Hg(II) and As(V) removal efficiencies were obtained, ensuring sufficient adsorption performance while maintaining experimental consistency throughout the study.

3.2.3 The kinetic behaviour of As(V) ions sorption by adsorbents

The kinetic parameters for As(V) adsorption onto CMR, CMG, and CMS are presented in Table 2 and Fig. 2d. The adsorption kinetics were analyzed using the pseudo-first-order and pseudo-second-order models in order to better understand the rate-controlling mechanisms governing the adsorption process.

For the pseudo-first-order model, the correlation coefficients (R^2) ranged from 0.989 to 0.996, whereas the pseudo-second-order model produced slightly lower values between 0.946 and 0.988. To further validate the goodness of fit, the sum of squared errors (SSE)

Table 2 Kinetic models of As (V) on different modified ceramic adsorbents

Kinetic Model	Parameter	CMR	CMG	CMS
Pseudo-first-order	(k_1) (min^{-1})	0.10	0.10	0.10
	(q_e) (mg g^{-1})	10.00	10.00	10.00
	(R^2)	0.989	0.989	0.996
	SSE	0.011	0.011	0.004
Pseudo-second-order	(k_2) (g mg^{-1} min^{-1})	0.548	0.586	0.842
	(h) (mg g^{-1} min^{-1})	0.183	0.174	0.182
	(q_e) (mg g^{-1})	0.485	0.472	0.464
	(R^2)	0.946	0.958	0.988
	SSE	0.054	0.042	0.012

was also evaluated. The pseudo-first-order model consistently produced lower SSE values (0.004–0.011) compared with the pseudo-second-order model (0.012–0.054). The combination of higher R^2 and lower SSE values indicates that the pseudo-first-order model provides a better representation of the experimental kinetic data.

A comparison between the experimental adsorption capacity $(q_{e,exp})$ and the calculated adsorption capacity $(q_{e,cal})$ further supports this observation, as the pseudo-first-order model shows closer agreement with the experimental values. This suggests that the adsorption rate is largely governed by the availability of active surface sites and concentration-dependent interactions between the adsorbate and the adsorbent surface.

Although the pseudo-second-order model also produced relatively high R^2 values, the comparatively higher SSE values indicate that it does not describe the adsorption kinetics as accurately as the pseudo-first-order model. Nevertheless, the reasonable fit of the pseudo-second-order model suggests that chemisorption processes, such as surface complexation or ion exchange, may still contribute partially to the adsorption mechanism.

Overall, the kinetic results indicate that As (V) adsorption on the ceramic materials is influenced by surface heterogeneity and multiple adsorbate–surface interactions. However, it should be noted that kinetic modeling alone cannot conclusively determine the adsorption mechanism, and both physical adsorption and chemical interactions may contribute to the overall removal process [30,31].

3.2.4 The effect of initial concentration

The heavy metal (Hg (II) affinity also affects the maximum adsorption capacity for various ions at presented in Table. The affinity of the adsorbed heavy metal ions was evaluated using the distribution of coefficient:

$$K_d = {}^{Q_e}/_{C_e} \tag{8}$$

In the equation K_d is the distribution coefficient that is used to express the ratio of equilibrium of the adsorption capacity of the adsorbent to the equilibrium concentration of the adsorbate (heavy metal ions in solution).

The distribution coefficient (K_d) values presented in Table 3 provide an indication of the affinity of the adsorbents for Hg(II) and As(V). In general, higher K_d values indicate stronger adsorption affinity and better removal potential. The results showed substantially higher K_d values for Hg(II) than for As(V), confirming that the ceramic materials had stronger affinity for mercury than for arsenate under the tested conditions [32].

Table 3 The distribution coefficient of CMS, CMR and CMG with Hg (II) and As(V)

C_0 (ppm) / K_d (L/Kg)		0.25	0.5	2.0	5.0	10.0
Hg (II)	CMS	625.83	690.82	379.53	214.22	144.59
	CMR	507.91	2443.44	233.46	159.38	48.46
	CMG	288.97	196.17	19.65	22.13	12.56
As (V)	CMS	6.53	4.19	2.04	1.71	1.66
	CMR	5.52	5.07	2.27	1.65	1.59
	CMG	5.90	3.73	1.99	1.67	1.59

This behavior is consistent with the greater tendency of divalent cationic Hg(II) species to interact with negatively charged or reactive surface sites on the ceramic matrices, whereas the adsorption of oxyanionic As(V) is less favorable at near-neutral pH. Also, the effect of initial Hg (II) and As (V) ion concentration in the range of 0.25–10 mg/L. It is clear that the adsorption capacity of the heavy metal decreases with the increase of initial ion concentration as indicated in Figs. 3a and b.

The results shows that the highest adsorption percentage of Hg (II) ions was 99.80 (CMR), 99.80 (CMS) and 99.71 (CMG); also, the highest percentage removal for As (V) ions is 84.67 (CMR), 85.51 (CMG) and 86.71 (CMS) at the initial Hg (II) and As (V) ion concentration of 0.25 mg/L. When all the active sites are involved in the adsorption process, the saturation and the maximum adsorbent capacity is achieved. Similar trend has been reported by [33] where the adsorption capacity of clay increased with the increase of initial metal ion concentration before attaining a plateau profile.

3.2.5 Adsorption isotherms of the materials

The adsorption isotherms describe the equilibrium distribution of Hg(II) and As(V) between the aqueous phase and the adsorbent surface. To better understand the adsorption behavior of the ceramic materials, the equilibrium data were analyzed using the

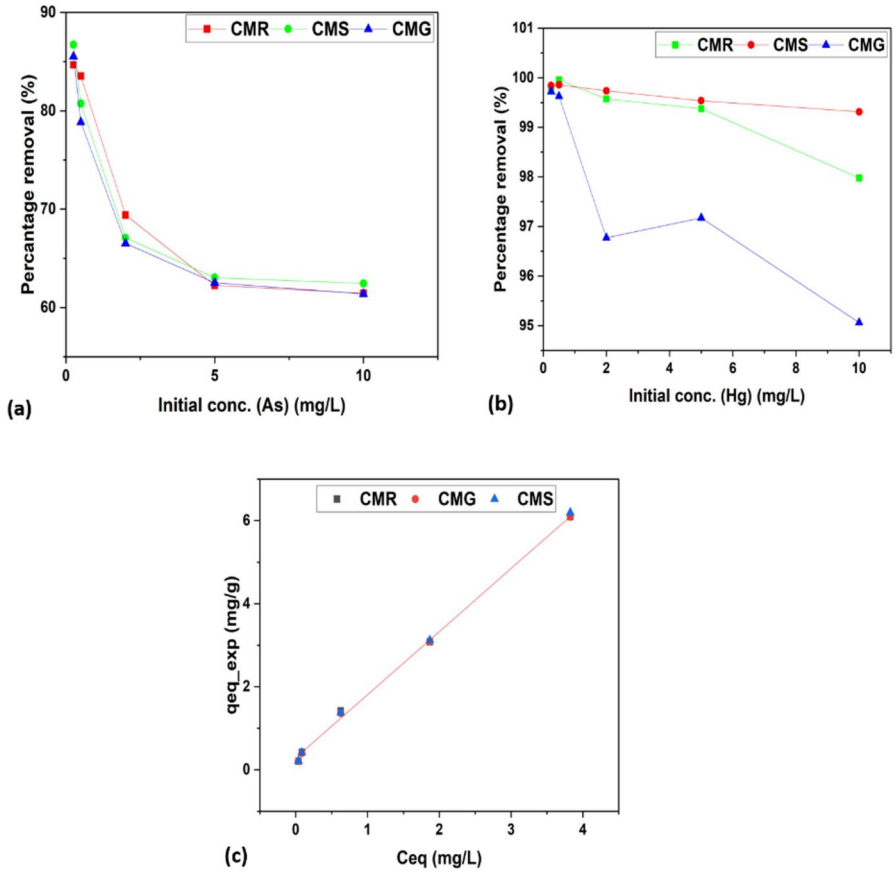

Fig. 3 **a** Effect of initial concentration of percentage removal of As (V), **b** Effect of initial concentration on removal of Hg (II) and **c** Adsorption equilibrium plot against equilibrium concentration

Table 4 Isotherms model parameters for the removal of Hg (II) ions from aqueous solution by adsorbents

Isotherm Model	Parameter	CMR	CMG	CMS
Freundlich	(n)	1.19	1.17	1.16
	(K_F) (mg g^{-1})	1.94	1.91	1.92
	(R^2)	0.997	0.993	0.996
	SSE	0.1038	0.0784	0.0895
Langmuir	(b) (L mg^{-1})	0.061	0.056	0.051
	(q_{max}) (mg g^{-1})	32.12	34.32	37.99
	(R^2)	0.992	0.994	0.994
	SSE	0.1856	0.1429	0.1528
Temkin	(A) (L mg^{-1})	18.04	17.76	17.74
	(B) (J mol^{-1})	6746.43	6740.99	6768.51
	(dQ) (J mg^{-1})	2251.21	2248.74	2216.65
	(R^2)	0.804	0.801	0.798
	SSE	4.6462	4.7668	5.0060

Freundlich, Langmuir, and Temkin isotherm models, and the corresponding parameters are summarized in Table 4.

For all three materials, the Freundlich model produced the highest correlation coefficients (R^2), ranging from 0.993 to 0.997, and the lowest sum of squared errors (SSE), with values between 0.0784 and 0.1038. The consistently lower SSE values further confirm that the Freundlich model provides the most accurate representation of the experimental equilibrium data. This indicates that Hg(II) adsorption occurs predominantly on heterogeneous surfaces with energetically non-uniform adsorption sites. The Freundlich constant K_F, which reflects adsorption capacity, showed similar values for the three materials (1.91–1.94 mg g^{-1}), suggesting comparable affinity of the ceramic matrices for Hg(II). In addition, the Freundlich heterogeneity factor n ranged from 1.16 to 1.19, with values greater than unity indicating favorable adsorption conditions and a strong interaction between Hg(II) ions and the adsorbent surfaces [34].

The Langmuir model also exhibited relatively high R^2 values (0.992–0.994), although the SSE values (0.1429–0.1856) were higher than those obtained for the Freundlich model. This suggests that monolayer adsorption may contribute to the overall adsorption process, but it does not fully capture the complexity of the heterogeneous ceramic surfaces. The Langmuir maximum adsorption capacity (q_{max}) values were calculated as 32.12, 34.32, and 37.99 mg g^{-1} for CMR, CMG, and CMS, respectively. The higher theoretical adsorption capacity observed for CMS indicates that the sheanut-shell-based ceramic material possesses a greater density of effective adsorption sites compared with the other materials.

In contrast, the Temkin model produced significantly lower R^2 values (0.798–0.804) and substantially higher SSE values (4.65–5.01), indicating poor agreement with the experimental data. These results suggest that the Temkin model is less suitable for describing the adsorption system under the investigated conditions.

Overall, the combined evaluation of R^2 and SSE confirms that the Freundlich isotherm best describes the equilibrium adsorption behavior of Hg(II) on the ceramic materials, supporting the presence of heterogeneous adsorption sites and multilayer adsorption

interactions. Such behavior is consistent with the structural complexity of clay-based ceramic matrices containing mixed mineral phases and irregular surface functional groups.

The adsorption behavior of Hg(II) and As(V) differed considerably due to their distinct aqueous speciation and interaction mechanisms with the ceramic surfaces. Hg(II), as a divalent cation, readily interacts with negatively charged surface sites through electrostatic attraction, surface complexation, and possible ion-exchange reactions. These interactions likely contribute to the higher removal efficiencies observed for mercury across all ceramic materials. In contrast, As(V) predominantly exists as oxyanionic species (such as $H_2AsO_4^-$ and $HAsO_4^{2-}$) under near-neutral pH conditions, which reduces its electrostatic affinity for the ceramic surfaces. Consequently, the adsorption of As(V) was consistently lower than that of Hg(II).

Among the tested materials, CMS exhibited the best adsorption performance. This improved behavior can be attributed to its higher amorphous fraction and smaller crystallite domains, as revealed by XRD analysis, which likely increased the availability of reactive surface sites and structural defects. These features promote stronger adsorbate–surface interactions and facilitate contaminant binding. Nevertheless, a more detailed understanding of the adsorption mechanisms would require post-adsorption characterization techniques such as SEM–EDS, FTIR, XPS, or XRD analysis of the spent adsorbents to identify possible surface complexation or structural changes occurring during adsorption.

3.3 Comparative study of adsorption during filtration and batch experiment

The adsorption performance of the three ceramic filter systems (CMR, CMS, and CMG) was further evaluated under filtration conditions for the removal of Hg(II) and As(V). The observed trends highlight the influence of biosorbent type, retention time, and ceramic microstructure on contaminant removal (Fig. 4).

For Hg(II), the CMS filter consistently outperformed the other materials, reaching nearly 70% removal after 24 h of filtration. In contrast, CMR and CMG showed lower removal efficiencies, plateauing at about 50%. The relatively rapid uptake by CMS suggests a greater availability of reactive binding sites and more favorable pore characteristics that promoted contaminant retention during flow-through operation. Thus, the order of filtration performance for Hg(II) was:

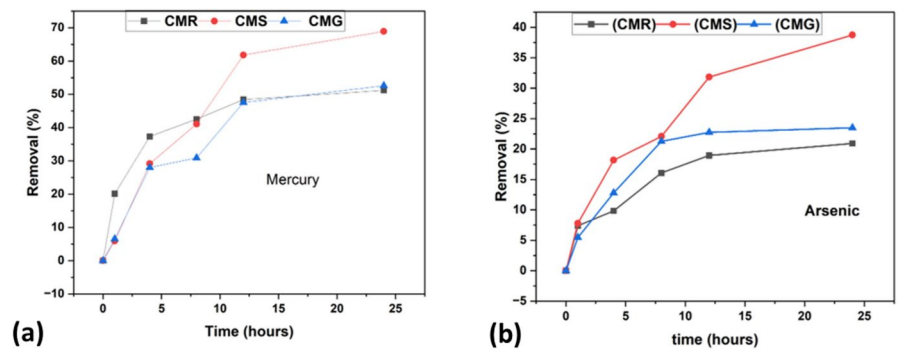

Fig. 4 Filtration capacity of different ceramic materials with **a** Hg (II) and **b** As (V)

$$CMS > CMR \approx CMG$$

For As(V), overall removal efficiencies were lower for all filters. CMS again showed the best performance, reaching approximately 38% removal after 24 h, followed by CMG and CMR. The comparatively lower adsorption of arsenic is likely related to its oxyanionic nature under neutral pH conditions, which reduces its affinity for the available adsorption sites relative to cationic Hg(II).

When compared with batch adsorption experiments, the filtration experiments generally produced lower removal efficiencies. This difference is most likely due to shorter effective contact times, mass-transfer limitations during flow-through operation, and incomplete utilization of adsorption sites under dynamic conditions. In contrast, batch experiments provide prolonged interaction between the adsorbate and adsorbent, resulting in greater uptake.

Overall, CMS exhibited the best adsorption and filtration performance for both Hg(II) and As(V), with particularly strong affinity toward Hg(II). These results suggest that sheanut-shell-modified ceramic filters are promising low-cost materials for point-of-use treatment of mercury-contaminated water, although further optimization will be needed to improve As(V) removal.

4 Conclusion

This study demonstrated the potential of locally fabricated ceramic water filters modified with agricultural biosorbents as low-cost adsorbents for the removal of Hg(II) and As(V) from contaminated water. Among the three formulations tested, the sheanut-shell-based ceramic material (CMS) exhibited the most favorable structural characteristics, including higher amorphous content and greater surface reactivity, which contributed to its superior adsorption performance.

Batch adsorption experiments showed that all adsorbents were capable of removing both Hg(II) and As(V), with CMS consistently outperforming CMR and CMG. The highest removal efficiencies were observed at lower initial concentrations, with maximum values of about 99.8% for Hg(II) and 86.7% for As(V). Kinetic analysis indicated that the pseudo-first-order model provided the best fit to the adsorption data, while equilibrium data were better described by the Freundlich isotherm model, suggesting adsorption on heterogeneous surfaces.

Under filtration conditions, CMS also achieved the best performance, with Hg(II) removal reaching about 70% and As(V) removal about 38% after 24 h. The lower efficiencies observed under filtration compared with batch conditions were attributed to reduced contact time and mass-transfer limitations. Although regeneration and reuse of spent filter materials are important considerations for sustainable water treatment, the present filtration system is intended for deployment in rural and resource-limited communities where users may have limited technical capacity for safe regeneration and handling of exhausted adsorbents. Improper reuse of spent filters may increase the risk of contaminant release and secondary contamination of drinking water. Therefore, the current study focuses on the filtration performance and practical applicability of the developed materials, while post-use management and regeneration strategies will be investigated in future studies. Overall, the results indicate that ceramic filters modified

with locally available biosorbents, particularly sheanut shells, offer a promising and accessible option for the treatment of mining-impacted water in rural and resource-constrained settings. Future work should investigate post-adsorption characterization, regeneration behavior, and additional surface modification strategies to improve arsenic removal and long-term performance.

Author contributions
Lydia Dziedzorm Senanu: Conceptualization, Methodology, Investigation, Writing—Original draft preparation Doris van Halem: Conceptualization, Methodology, Supervision, Writing—Reviewing and Editing Gordana Kranjac-Berisavljevic: Conceptualization, Supervision, Writing—Reviewing and Editing Samuel Jerry Cobbina: Conceptualization, Supervision, Writing—Reviewing and Editing Bas Heijman: Conceptualization, Methodology, Supervision, Writing—Reviewing and Editing Bennet Edem Akorley Investigation,Writing—Reviewing and Editing.

Funding
The authors did not receive any funding.

Data availability
All materials, data and software applications support our claims and comply with field standards.

Declarations

Ethics approval and consent to participate
Not applicable. This study did not involve human participants, animals, or clinical samples.

Consent for publication
Not applicable.

Competing interests
The authors declare no competing interests.

Received: 10 January 2026 Accepted: 15 July 2026
Published online: 03 August 2026

References

1. Niazi NK, Bibi I, Shahid M, Ok YS, Shaheen SM, Rinklebe J, et al. Arsenic removal by Japanese oak wood biochar in aqueous solutions and well water: investigating arsenic fate using integrated spectroscopic and microscopic techniques. Sci Total Environ. 2018;621:1642–51. https://doi.org/10.1016/j.scitotenv.2017.10.063.
2. Sharma A, Sharma A, Arya RK. Removal of mercury (II) from aqueous solution: a review of recent work. Sep Sci Technol. 2015;50(9):1310–20. https://doi.org/10.1080/01496395.2014.968261.
3. Mkwate RC, Chidya RCG, Wanda EMM. Assessment of drinking water quality and rural household water treatment in Balaka District, Malawi. Phys Chem Earth, Parts A/B/C. 2017;100:353–62. https://doi.org/10.1016/j.pce.2016.10.006.
4. Awotwi A, Anornu GK, Quaye-Ballard JA, Annor T, Nti IK, Odai SN, et al. Impact of post-reclamation of soil by large-scale, small-scale and illegal mining on water balance components and sediment yield: Pra River Basin case study. Soil Tillage Res. 2021;211:105026. https://doi.org/10.1016/j.still.2021.105026.
5. Bansah KJ, Dumakor-Dupey NK, Kansake BA, Assan E, Bekui P. Socioeconomic and environmental assessment of informal artisanal and small-scale mining in Ghana. J Clean Prod. 2018;202:465–75. https://doi.org/10.1016/j.jclepro.2018.08.150.
6. Cobbina SJ, Nkuah D, Tom-Dery D, Obiri S. Non-cancer risk assessment from exposure to mercury (Hg), cadmium (Cd), arsenic (As), copper (Cu) and lead (Pb) in boreholes and surface water in Tinga, in the Bole-Bamboi District, Ghana. J Toxicol Environ Health Sci. 2013;5(2):29–36. https://doi.org/10.5897/JTEHS12.0253.
7. Karikari AY, Duah AA, Akurugu BA, Darko HF. Assessing the impacts of artisanal mining on the quality ofvf South-western Rivers System in Ghana. Environ Monit Assess. 2021. https://doi.org/10.1007/s10661-021-09515-y.
8. Smedley PL, Kinniburgh DG. A review of the source, behaviour and distribution of arsenic in natural waters. Appl Geochem. 2002;17(5):517–68. https://doi.org/10.1016/S0883-2927(02)00018-5.
9. Mondal MK, Garg R. A comprehensive review on removal of arsenic using activated carbon prepared from easily available waste materials. Environ Sci Pollut Res. 2017;24(15):13295–306. https://doi.org/10.1007/s11356-017-8842-7.
10. Robbins EC, Guo J, Adams CD. Removal of As (III) and As (V) in surface modified ceramic filters. J Water Sanit Hyg Dev. 2014;4(2):214–22. https://doi.org/10.2166/washdev.2014.114.
11. Shakoor MB, Niazi NK, Bibi I, Rahman MM, Naidu R, Dong Z, et al. Unraveling health risk and speciation of arsenic from groundwater in rural areas of Punjab, Pakistan. Int J Environ Res Public Health. 2015;12(10):12371–90. https://doi.org/10.3390/ijerph121012371.
12. Bibi S, Farooqi A, Yasmin A, Kamran MA, Niazi NK. Arsenic and fluoride removal by potato peel and rice husk (PPRH) ash in aqueous environments. Int J Phytoremediation. 2017;19(11):1029–36. https://doi.org/10.1080/15226514.2017.1319329.

13. Mohanty D. Conventional as well as emerging arsenic removal technologies—a critical review. Water Air Soil Pollut. 2017;228(10):1–21. https://doi.org/10.1007/s11270-017-3549-4.
14. LeMonte JJ, Stuckey JW, Sanchez JZ, Tappero R, Rinklebe J, Sparks DL. Sea level rise induced arsenic release from historically contaminated coastal soils. Environ Sci Technol. 2017;51(11):5913–22. https://doi.org/10.1021/acs.est.6b06152.
15. Niazi NK, Burton ED. Arsenic sorption to nanoparticulate mackinawite (FeS): an examination of phosphate competition. Environ Pollut. 2016;218:111–7. https://doi.org/10.1016/j.envpol.2016.08.031.
16. Blue LY. Immobilization of mercury and arsenic through covalent thiolate bonding for the purpose of environmental remediation. University of Kentucky; 2010.
17. Arai Y, Elzinga EJ, Sparks DL. X-ray absorption spectroscopic investigation of arsenite and arsenate adsorption at the aluminum oxide–water interface. J Colloid Interface Sci. 2001;235(1):80–8. https://doi.org/10.1006/jcis.2000.7249.
18. Krstić V, Urošević T, Pešovski B. A review on adsorbents for treatment of water and wastewaters containing copper ions. Chem Eng Sci. 2018;192:273–87. https://doi.org/10.1016/j.ces.2018.07.022.
19. Rad LR, Anbia M. Zeolite-based composites for the adsorption of toxic matters from water: a review. J Environ Chem Eng. 2021;9(5):106088. https://doi.org/10.1016/j.jece.2021.106088.
20. de Gennaro B, Aprea P, Liguori B, Galzerano B, Peluso A, Caputo D. Zeolite-rich composite materials for environmental remediation: arsenic removal from water. Appl Sci. 2020;10(19):6938. https://doi.org/10.3390/app10196939.
21. Sullivan RK, Erickson M, Oyanedel-Craver VA. Understanding the microbiological, organic and inorganic contaminant removal capacity of ceramic water filters doped with different silver nanoparticles. Environ Sci Nano. 2017;4(12):2348–55. https://doi.org/10.1039/C7EN00443E.
22. Agrawal VK, Bhalwar R. Household water purification: low-cost interventions. Med J Armed Forces India. 2009;65(3):260–3. https://doi.org/10.1016/S0377-1237(09)80019-1.
23. Farrow C, McBean E, Huang G, Yang A, Wu Y, Liu Z, et al. Ceramic water filters: a point-of-use water treatment technology to remove bacteria from drinking water in Longhai City, Fujian Province. China J Environ Inform. 2018;32(2):63–8. https://doi.org/10.3808/jei.201800388.
24. Ali A, Ahmed A, Gad A. Chemical and microstructural analyses for heavy metals removal from water media by ceramic membrane filtration. Water Sci Technol. 2017;75(2):439–50. https://doi.org/10.2166/wst.2016.537.
25. Pérez-Vidal A, Silva-Leal JA, Diaz-Gómez J, Meneses-Torres CJ, Arias-Vallejo JE, Giraldo-Tenorio GA, et al. Performance evaluation of ceramic pot filters combined with adsorption processes for the removal of heavy metals and phenolic compounds. J Water Health. 2021;19(5):750–61. https://doi.org/10.2166/wh.2021.052.
26. Nigay P-M, Salifu AA, Obayemi JD, White CE, Nzihou A, Soboyejo WO. Ceramic water filters for the removal of bacterial, chemical, and viral contaminants. J Environ Eng. 2019;145(10):04019066. https://doi.org/10.1061/(ASCE)EE.1943-7870.0001579.
27. Yang X, Huang G, An C, Chen X, Shen J, Yin J, et al. Removal of arsenic from water through ceramic filter modified by nano-CeO2: a cost-effective approach for remote areas. Sci Total Environ. 2021;750:141510.
28. Apea OB, Akorley BE, Oyelude EO, Ampadu B. Evaluation of the adsorption behavior and divalent metal ions removal efficiency of ceramic point-of-use water filter materials. Environ Syst Res. 2023;12(1):37. https://doi.org/10.1186/s40068-023-00322-7.
29. Padmavathy KS, Madhu G, Haseena PV. A study on effects of pH, adsorbent dosage, time, initial concentration and adsorption isotherm study for the removal of hexavalent chromium (Cr (VI)) from wastewater by magnetite nanoparticles. Procedia Technol. 2016;24:585–94. https://doi.org/10.1016/j.protcy.2016.05.127.
30. Revellame ED, Fortela DL, Sharp W, Hernandez R, Zappi ME. Adsorption kinetic modeling using pseudo-first order and pseudo-second order rate laws: a review. Clean Eng Technol. 2020;1:100032. https://doi.org/10.1016/j.clet.2020.100032.
31. Wong YC, Szeto YS, Cheung WH, McKay G. Equilibrium studies for acid dye adsorption onto chitosan. Langmuir. 2003;19(19):7888–94. https://doi.org/10.1021/la030064y.
32. Ahmad M, Lee SS, Dou X, Mohan D, Sung J-K, Yang JE, et al. Effects of pyrolysis temperature on soybean stover-and peanut shell-derived biochar properties and TCE adsorption in water. Bioresour Technol. 2012;118:536–44. https://doi.org/10.1016/j.biortech.2012.05.042.
33. Abbou B, Lebkiri I, Ouaddari H, Elkhattabi O, Habsaoui A, Lebkiri A, et al. Kinetic and thermodynamic study on adsorption of cadmium from aqueous solutions using natural clay. J Turkish Chem Soc Sect A: Chem. 2021;8(2):677–92. https://doi.org/10.18596/jotcsa.882016.
34. Dada AO, Ojediran JO, Olalekan AP. Sorption of Pb 2 + from aqueous solution unto modified rice husk: isotherms studies. Adv Phys Chem. 2013. https://doi.org/10.1155/2013/842425.
35. Park JD, Zheng W. Human exposure and health effects of inorganic and elemental mercury. J Prev Med Public Health. 2012;45(6):344. https://doi.org/10.3961/jpmph.2012.45.6.344.
36. Shakir SK, Azizullah A, Murad W, Daud MK, Nabeela F, Rahman H, et al. Toxic metal pollution in Pakistan and its possible risks to public health. In: Reviews of environmental contamination and toxicology volume 242. Cham: Springer International Publishing; 2016. p. 1–60. https://doi.org/10.1007/398_2016_9.
37. Shi G, Chen Z, Teng J, Bi C, Zhou D, Sun C, et al. Fluxes, variability and sources of cadmium, lead, arsenic and mercury in dry atmospheric depositions in urban, suburban and rural areas. Env Res. 2012;113:28–32.
38. Zhuang W, Gao X. Distributions, sources and ecological risk assessment of arsenic and mercury in the surface sediments of the southwestern coastal Laizhou Bay, Bohai Sea. Mar Pollut Bull. 2015;99(1–2):320–7. https://doi.org/10.1016/j.marpolbul.2015.07.037.
39. Jennrich P. The influence of arsenic, lead, and mercury on the development of cardiovascular diseases. Int Sch Res Not. 2013;2013(1):234034. https://doi.org/10.5402/2013/234034.
40. Abarikwu SO. Lead, arsenic, cadmium, mercury: occurrence, toxicity and diseases. In: Pollutant diseases, remediation and recycling. Cham: Springer International Publishing; 2013. p. 351–86. https://doi.org/10.1007/978-3-319-02387-8_7.

41. Wróblewski M, Miłek J, Godlewski A, Wróblewska J. The impact of arsenic, cadmium, lead, mercury, and thallium exposure on the cardiovascular system and oxidative mechanisms in children. Curr Issues Mol Biol. 2025;47(7):483. https://doi.org/10.3390/cimb47070483.
42. Teschke R, Xuan TD. Heavy metals like aluminum, arsenic, cadmium, chromium, copper, iron, lead, manganese, mercury, nickel, and zinc polluting the drinking water: their individual health hazards. Int J Mol Sci. 2025;26(23):11656. https://doi.org/10.3390/ijms262311656.
43. Bielefeldt AR, Kowalski K, Schilling C, Schreier S, Kohler A, Summers RS. Removal of virus to protozoan sized particles in point-of-use ceramic water filters. Water Res. 2010;44(5):1482–8. https://doi.org/10.1016/j.watres.2009.10.043.
44. Simonis JJ, Basson AK. Evaluation of a low-cost ceramic micro-porous filter for elimination of common disease microorganisms. Phys Chem Earth, Parts a/b/c. 2011;36(14–15):1129–34. https://doi.org/10.1016/j.pce.2011.07.064.
45. Rivera-Sánchez SP, Ocampo-Ibáñez ID, Silva-Leal JA, Flórez-Elvira LJ, Castaño-Hincapié AV, Dávila-Estupiñan A, et al. A novel filtration system based on ceramic silver-impregnated pot filter combined with adsorption processes to remove waterborne bacteria. Sci Rep. 2020;10(1):11198.
46. Shafiquzzaman M, Hasan MM, Haider H, Bari QH, EL-Ghoul Y, Nakajima J. Arsenic removal by household-based ceramic filters: evaluating mode of operations and influence of groundwater compositions. J Water Process Eng. 2022;46:102598. https://doi.org/10.1016/j.jwpe.2022.102598.
47. Jana S, Saikia A, Purkait MK, Mohanty K. Chitosan based ceramic ultrafiltration membrane: preparation, characterization and application to remove Hg (II) and As (III) using polymer enhanced ultrafiltration. Chem Eng J. 2011;170(1):209–19. https://doi.org/10.1016/j.cej.2011.03.056.
48. Kurniawan TA, Lo W, Liang X, Goh HH, Othman MHD, Chong KK, et al. Remediation technologies for contaminated groundwater due to arsenic (As), mercury (Hg), and/or fluoride (F): a critical review and way forward to contribute to carbon neutrality. Sep Purif Technol. 2023;314:123474. https://doi.org/10.1016/j.seppur.2023.123474.
49. Alkhudhiri A, Hakami M, Zacharof MP, Abu Homod H, Alsadun A. Mercury, arsenic and lead removal by air gap membrane distillation: experimental study. Water. 2020;12(6):1574. https://doi.org/10.3390/w12061574.
50. Ng KS, Ujang Z, Le-Clech P. Arsenic removal technologies for drinking water treatment. Rev Environ Sci Biotechnol. 2004;3(1):43–53. https://doi.org/10.1023/B:RESB.0000040054.28151.84.

Publisher's Note